Eurasian Journal of Analytical Chemistry
ISSN: 1306-3057 OPEN ACCESS 2024 19 (1): 54-64

Designing Of Slns Encapsulating Busulfex Association In Gene Polymorphism And Its Treatment Outcome For Head And Neck Cancer

Garima Avasthi[1*], Dr.Amresh Gupta[2],Dr.Devendra Parmar[3]

[1*,2]Goel Institute of Pharmacy and Sciences, Lucknow
[3]Indian Institute of Toxicology and Research, Lucknow

***Corresponding Author:** Garima Avasthi
*Goel Institute of Pharmacy and Sciences, Lucknow

Abstract
This research is dedicated to the creation and analysis of Chitosan Nanoparticles loaded with Busulfan for potential medical applications. The main goal was to produce nanoparticles with specific physical and chemical properties and a sustained release of the drug. Nine different formulations (CNB-1 to CNB-9) were developed using varying concentrations of chitosan and tripolyphosphate (TPP) via a method called ionic gelation. The nanoparticles underwent extensive testing for their size distribution, electrical charge, drug entrapment efficiency, drug content, and how the drug was released over time in vitro. The results showed that CNB-4 had the most desirable characteristics, with an average size of 172 ± 2 nanometers, a slight positive charge (4 ± 1 millivolts), high drug entrapment, and a slow release of the drug over 24 hours. Further examination using techniques like Differential Scanning Calorimetry (DSC) and Atomic Force Microscopy (AFM) confirmed that CNB-4 was successfully formed and had a solid structure. DSC analysis showed no interactions between the drug and the polymer, while AFM images displayed dense, spherical nanoparticles. Over the course of 24 hours, CNB-4 released almost 90% of the therapeutic payload, according to in vitro release assays, demonstrating a continuous release of the medication. Statistical analysis revealed a strong correlation between the physical and chemical properties of the formulations and their release rates. In conclusion, CNB-4's favourable features made it an attractive prospect for controlled drug delivery in treatment for cancer. The findings of this study can be used to enhance drug delivery systems that rely on nanoparticles and to better understand how to optimise formulation parameters to achieve desired therapeutic effects.

Keywords*:* Busulfan, Solid Lipid Nanoparticles, drug encapsulation, cancer treatment.

Introduction

Cancer, a complex and devastating disease, continues to pose significant challenges to global health, affecting millions of lives worldwide each year. Despite considerable progress in cancer research and treatment, current therapeutic approaches such as chemotherapy, surgery, and radiation therapy are accompanied by substantial limitations, including systemic toxicity, drug resistance, and off-target effects. These challenges underscore the urgent need for innovative strategies that can overcome these barriers and improve the efficacy and safety of cancer treatment. In recent years, nanotechnology has emerged as a promising frontier in cancer therapy, offering unprecedented opportunities for targeted drug delivery, enhanced therapeutic efficacy, and reduced side effects. By harnessing the unique properties of nanomaterials, researchers have developed a diverse array of nanocarriers capable of delivering therapeutic agents specifically to cancer cells while sparing healthy tissue. Due to their inherent benefits and adaptability, Solid Lipid Nanoparticles (SLNs) received substantial attention among the numerous nanocarriers studied for cancer treatment delivery. Composed of biocompatible lipids, SLNs offer several distinct advantages as drug delivery vehicles, including excellent stability, controlled release kinetics, and the ability to encapsulate a wide range of hydrophobic and hydrophilic drugs. Moreover, SLNs can be surface-modified with targeting ligands or functional groups to enhance their specificity and affinity for cancer cells, thereby minimizing systemic exposure and off-target effects. Previous research in the field of nanomedicine has demonstrated the potential of SLNs in improving the pharmacokinetics, biodistribution, and therapeutic efficacy of anticancer drugs, paving the way for their translation into clinical applications. The rationale for using SLNs in cancer treatment is multifaceted and supported by a growing body of evidence. To begin with, SLNs can overcome formulation problems and increase the therapeutic efficacy of medications by improving their solubility and bioavailability. This is especially true for weakly water-soluble pharmaceuticals, including many anticancer treatments. Secondly, SLNs possess the ability to encapsulate drugs within their lipid matrix, protecting them from degradation and premature release in systemic circulation, while facilitating their targeted delivery to tumor sites through passive or active mechanisms. Another advantage of SLNs is their adaptability; they can be

made to have longer circulation periods in the blood, which means the medicine may be released slowly but steadily, and it can accumulate better in tumours because of the EPR effect. Furthermore, the development of SLNs as drug delivery systems offers the potential to address some of the key limitations associated with conventional cancer treatments. By encapsulating cytotoxic drugs within SLNs, it is possible to minimize systemic toxicity and off-target effects, thereby improving the therapeutic index and patient tolerability. Moreover, SLNs have been shown to overcome multidrug resistance mechanisms in cancer cells, making them particularly attractive for the treatment of drug-resistant malignancies. The ability of SLNs to encapsulate a combination of therapeutic agents, such as chemotherapy drugs and molecularly targeted agents, also holds promise for overcoming tumor heterogeneity and improving treatment outcomes in patients with advanced or metastatic disease. Against this backdrop, the research objective of this study is to develop and analyze SLNs encapsulating Busulfex (Busulfan), a widely used alkylating agent in the treatment of hematologic malignancies such as leukemia and lymphoma. Busulfex exhibits potent anticancer activity but is limited by its poor aqueous solubility, rapid clearance, and dose-limiting toxicity, highlighting the need for innovative delivery strategies to enhance its therapeutic efficacy and minimize side effects. By encapsulating Busulfex within SLNs, we aim to address these challenges and optimize its pharmacokinetic profile, biodistribution, and tumor-targeting efficiency, ultimately improving its therapeutic index and clinical utility in cancer treatment. This study's importance rests in the fact that it may lead to new insights on the use of SLN-based drug delivery systems in cancer treatment. By elucidating the mechanisms underlying the pharmacokinetics, biodistribution, and therapeutic efficacy of SLN-encapsulated Busulfex, this study aims to inform the development of more effective and personalized treatment strategies for patients with hematologic malignancies. Further, this research may contribute to the ongoing efforts to improve patient care and outcomes by providing insights into the development and optimization of SLN-based formulations for other anticancer drugs and therapeutic modalities.

Materials and Methods

Materials

Busulfan, as well as surfactants (such as Polysorbate 80 and Poloxamer 188), solvents (such as ethanol and acetone), and excipients (such as Polyethylene glycol, Tween 20) are the components of SLNs containing Busulfan. Various chemicals are used in the preparation of buffer solutions (such as phosphate-buffered saline, pH 7.4), lipids (such as stearic acid), and other substances (such as sodium hydroxide and hydrochloric acid). To achieve successful drug encapsulation and delivery in cancer treatment, it is imperative that all the constituents of the SLN formulation be carefully selected and optimized in order to achieve its optimal structure, stability, and efficacy.

Method

Preformulation Studies

FTIR spectroscopy

Busulfan hydrochloride, chitosan, and a physical mixture (in a 1:1 ratio) of Busulfan hydrochloride and chitosan were mixed with anhydrous potassium bromide (KBr) at a 1:4 ratio as part of the study. 100 mg of fine powder were crushed into KBr pellets using a TechnoSearch hydraulic press set at 15 tons of pressure. A Fourier transform infrared spectrophotometer was used to scan the pellets for wave numbers of 400 cm-1 to 4000 cm-1. We used the infrared peak matching method to compare the IR spectrum of the physical mixture to that of pure Busulfan hydrochloride and chitosan in order to determine whether specific peaks existed.

Differential Scanning Calorimetry

Thermal properties of Busulfan hydrochloride were evaluated by mixing Busulfan hydrochloride with chitosan, a physical mixture, and chitosan nanoparticles. A crated aluminum pan contains precisely measured samples measuring between 3 and 5 milligrams. Differential scanning calibration (DSC) was used to obtain thermograms by heating them at 10 degrees C per minute. We use a constant nitrogen flow at temperatures of 20 to 300°C as the filtration gas, while there is an empty reference sheet. The DSC thermograms of Busulfan hydrochloride, chitosan, and physical mixtures (1:1), as well as chitosan nanoparticles loaded with Busulfan hydrochloride, were collected and analyzed with TA universal analysis.

Preparation of busulfan loaded nanoparticles by ionic gelation method
Ion gels have been used to synthesize chitosan nanoparticles filled with busulfan hydrochloride (CS-NP). A mixture of chitosan (0.3%, 0.5% and 0.7%) was dissolved in glacier acetic acid at a concentration of 1%. The solution was then continuously mixed with a magnetic mixer and added 7 mg Busulfan hydrochloride. The mixture was then slowly drained at concentrations of 0.3%, 0.5% and 0.7% in Tripoliphosphate (TPP). We stirred the suspension magnetically for 35 minutes and sounded for 35 minutes. To eliminate excess TPP and intact Busulfan, a 15 000 rpm, 5°C ultracentrifuge was used to centrifuge the nanoparticle suspension for 35 minutes at 14 000 rpm. After dispersing the pellets into deionized water, a freeze dryer was used to lyophilize the powder for two days.

Enhancing Busulfan Nanoparticles with Hyaluronic Acid Conjugation
The preparation of hyaluronic acid-conjugated nanoparticles employed a technique based on electrostatic attraction. Initially, a 1 ml dispersion of nanoparticles containing Busulfan hydrochloride was meticulously introduced into solutions comprising hyaluronic acid at concentrations of 0.10% and 0.20%. This process involved a gradual addition of the nanoparticle dispersion to the hyaluronic acid solutions, ensuring thorough mixing throughout. The concentration of hyaluronic acid as well as the rate of addition of nanoparticles were considered during an analysis after confirming that the nanoparticle dispersion was correct. These variables were meticulously examined to ascertain the most favorable conditions for achieving the optimal formulation.

Characterization of busulfan-prepared nanoparticles

Analysis of Particle Size Distribution and Polydispersity Index
Nanoparticle homogeneity and size were measured using the Zetasizer ZS 90 device using dynamic light scattering (DLS). The device uses a 576nm wavelength laser placed at 45° angle in a 21mm diameter cell. It operates at a temperature of 53 degrees C. The DLS uses Brown motion to measure particle movement and applies the Stokes–Einstein equation to calculate particle size distribution. Measurements were carried out on five occasions to determine the average particle size of the nanoparticles, and results are presented as standard deviation for average diameter.

Determination of Zeta Potential
To analyze the zeta potential of nanoparticles, ZetaSizer ZS90 is used and the Helmholtz–Smoluchowski equation is used to determine values. After sonication in the bath sonicator, the Busulfan nanoparticles are dispersed in 2 ml double-distilled water to ensure uniform dispersion. Zeta dip cells and disposable polystyrene cuvettes were used for the measurements at 37°C. A standard deviation of the average diameter was calculated for each measurement after performing it five times.

Characterization of Formulated busulfan Nanoparticles

Transmission electron microscopy (TEM)
The work focused on examining the physical structure of the nanoparticles containing Busulfan. The goal of this study was the use of Transmission Electron Microscopy (TEM) operated at 100 kV. TEM images were then taken under low vacuum conditions using the copper grid containing the dehydrated nanosuspension, and subsequently recorded for further research.

Entrapment efficiency
Entrapment efficiency, a critical parameter in nanoparticle formulation, was determined through a rigorous process. The encapsulated Busulfan was separated from the formulation via ultracentrifugation for 45 minutes at 13000 rpm at 4°C. Following centrifugation, the supernatants, which contained any residual Busulfan, were carefully collected. A UV spectrophotometer was used to precisely calculate the entrapment efficiency of the nanoparticles by quantifying the concentration of Busulfan in the supernatants.

Entrapment Efficiency (%) = [(Total amount of drug or compound - Amount of unentrapped substance) / Total amount of drug or compound] x 100
% Yield of Nanoparticles
Prepare nanoparticle formulation. Subject to centrifugation to separate nanoparticles. Collect and measure nanoparticle pellet weight. Calculate yield as a percentage of initial nanoparticle amount.

Nanoparticle Yield (%) = (Weight of nanoparticle pellet / Initial nanoparticle amount) x 100
% Drug loading
A critical step in evaluating the medicinal properties of Busulfan nanoparticles was their encapsulation. At first, 40 mg freeze-dried nanoparticles were carefully dissolved in acetonitrile. A thorough evaluation of the drug

loading efficiency was then conducted using ultraviolet spectroscopy to measure the drug concentration accurately.

Concentration (mg/ml) = Amount of drug (mg)\Volume of solvent (ml)

Studies on the release of drugs in vitro

In vitro release tests were conducted with the dialysis technical bag. We freeze-dried 2 milligrams of busulfan nanoparticles encapsulated in a dialysis membrane with a molecular weight cutoff of 10,000–12,000 Da. With membrane clips, the membrane was secured securely. For immersing the membrane, a pH 7.4 phosphate buffer solution was used. The beaker was maintained at a temperature of 37 degrees Celsius and stirred continuously using a magnetic stirrer. We collected 2 millilitre samples from the solution at certain time intervals (one, two, four, eight, twelve, and twenty-four hours) and replaced them with an equivalent volume of fresh pH 7.4 phosphate buffer solution. A spectrophotometric analysis was used to determine busulfan concentration.

Results and Discussion

Preformulation Studies

FT-IR spectroscopy

To explore if Busulfan, Chitosan, or their combination are physically or chemically interconnected, Fourier-transform infrared spectroscopy was used. According to the FT-IR spectrum of the physical mixture, no new peaks or disappearance of existing peaks were observed, confirming busulfan's compatibility with Chitosan. Table 7.1 provides the infrared absorption values for the individual components and the physical mixture, while Figure 1, 2 and 3 illustrates the corresponding FT-IR spectra.

The provided table summarizes the infrared spectroscopy findings concerning the distinctive functional groups present in Busulfan, chitosan, and their physical combination. Variations in peak wave numbers suggest differing molecular structures and bonding environments across the components. For instance, discrepancies in OH group peak wave numbers hint at diverse hydrogen bonding situations. Similarly, differences in CH stretching vibrations and C=O stretching peak wave numbers imply structural dissimilarities among the compounds. The identification of NH2 stretching vibrations solely in chitosan suggests the presence of amino groups. Furthermore, disparities in peak wave numbers for C-O-C groups highlight varying ether linkages. Intriguingly, the detection of a β-1-4 glycosidic linkage peak in the physical blend indicates potential interactions between Busulfan and chitosan. In summary, these spectroscopic outcomes offer insights into the chemical attributes and potential interactions of the examined substances, shaping their application in pharmaceutical formulations. Further examination and interpretation of these results can enhance our understanding of the behavior of these substances in pharmaceutical contexts.

Table 1 Infrared spectroscopy analysis of busulfan, chitosan, and their physical mixture

Functional Groups	Peak Wave Number (cm^-1)	Busulfan	Chitosan	Physical Mixture
OH	3380.21	3374.39	3358.54	-
CH Stretch	2964.87	2922.79	2926.15	-
C=O Stretching	1610.77	1681.49	1613.27	-
NH2 (C-N Stretching)	-	1155.27	1191.89	-
C-O-C	1036.49	1025.14	1013.86	-
β-1-4 Glycosidic Linkage	-	-	808.33	852.12

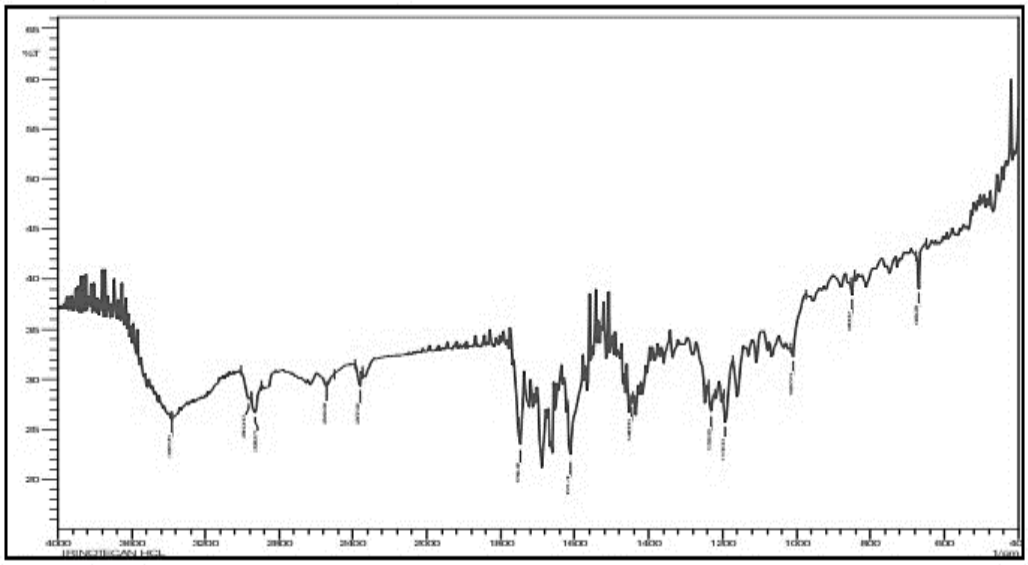

Figure 1 Infrared absorption spectrum of Pure Busulfan

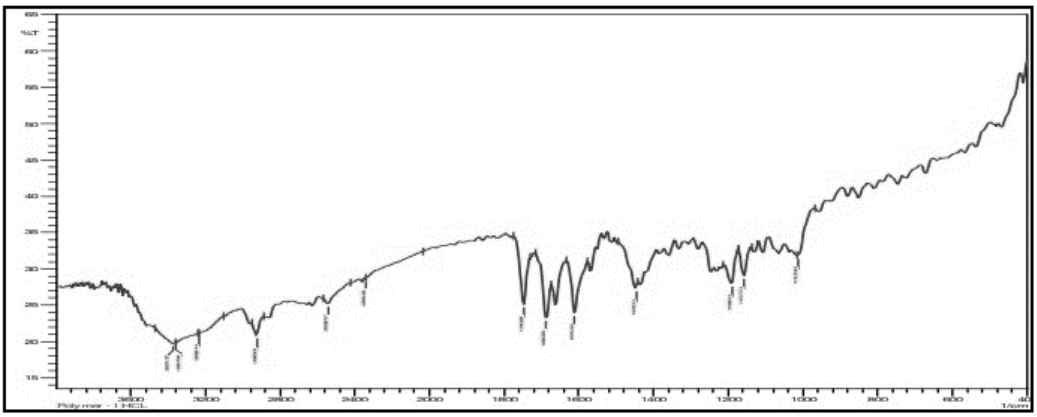

Figure 2 Infrared absorption spectrum of Chitosan

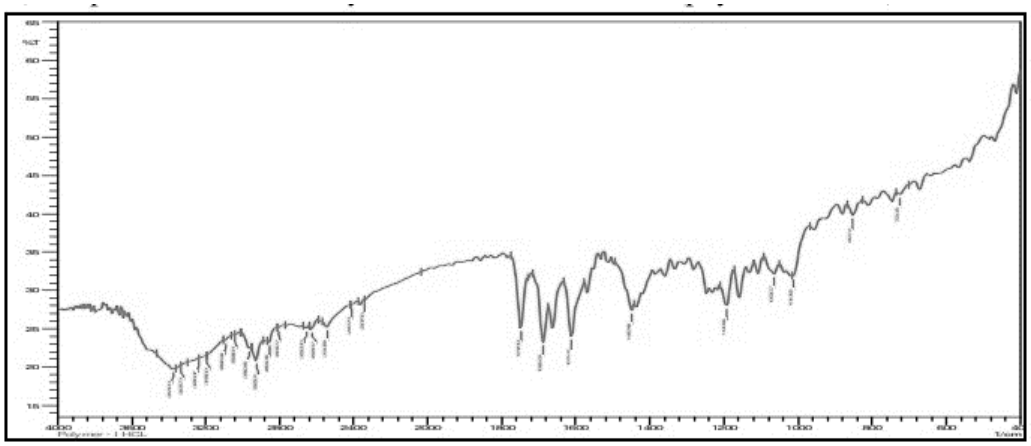

Figure 3 Infrared absorption spectrum of physical mixture

Differential Scanning Calorimetry

The study employed differential scanning calorimetry (DSC) to examine potential interactions among Busulfan, chitosan, the physical mix, and chitosan nanoparticles containing Busulfan (CS-NPs). The examination of the DSC thermograms revealed distinct and well-defined endothermic peaks at temperatures of 285.23°C and 339.47°C for Busulfan and chitosan, respectively. Upon combining Busulfan with chitosan in a physical blend, we found endothermic peaks that represented the crystalline character and compatibility of both components. A reduction in the peak intensity of busulfan in the loaded nanoparticles indicated the presence of the drug in an amorphous state. The DSC overlay image, depicted in Figure 4, visually illustrates these findings. This analysis provides

insights into the thermal behavior and compatibility of the studied components, which are essential considerations for the development of pharmaceutical formulations.

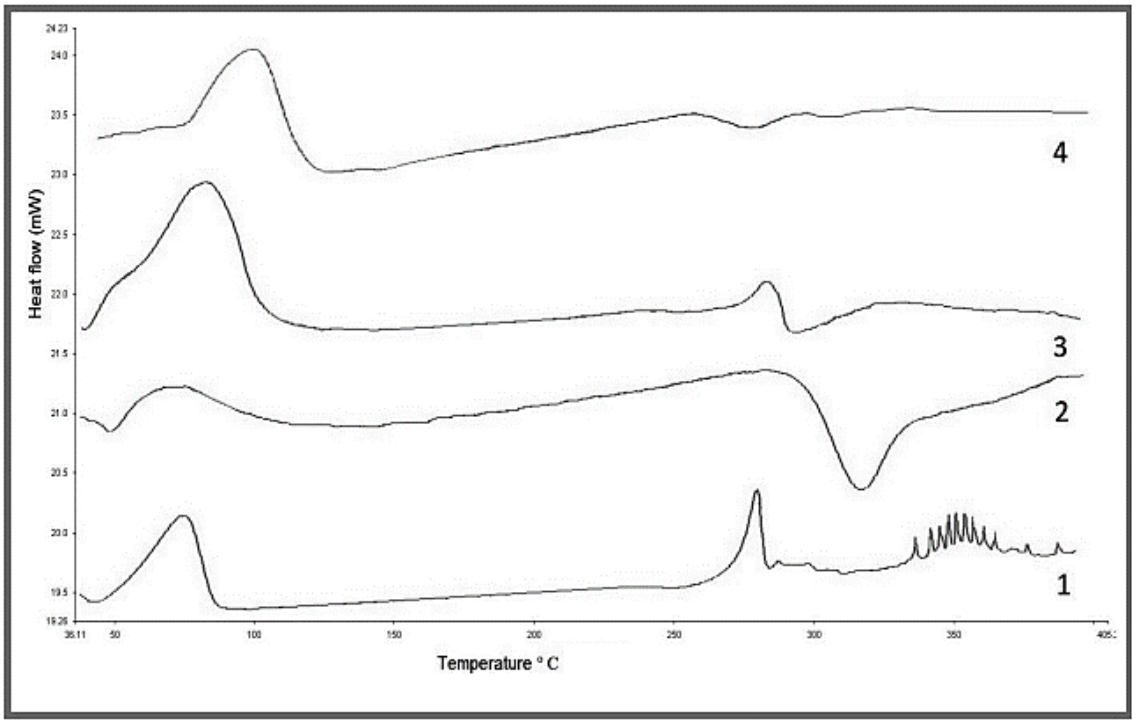

Figure 4 Comparison of DSC Thermograms for A) Busulfan, B) Chitosan, C) Physical Mixture of Busulfan and Chitosan, and D) Nanoparticle Formulation of Busulfan with Chitosan

Preparation of busulfan loaded Chitosan nanoparticles by solvent evaporation method

The process of creating Busulfan-loaded chitosan nanoparticles involved the implementation of the ionic gelation method, which consisted of the following sequential steps: To begin, a 1% weight/volume chitosan solution was created by dissolving chitosan powder in acetic acid while continuously stirring until the chitosan powder was completely dissolved. Concurrently, a solution of sodium tripolyphosphate (TPP) with a concentration of 0.5% weight/volume (w/v) was created by dissolving TPP powder in water that had been distilled twice. Subsequently, the Busulfan solution was incrementally introduced into the chitosan solution with continuous stirring to guarantee comprehensive blending. Afterwards, the TPP solution was slowly added while vigorously swirling. The concoction was agitated for an extra 30 minutes to enhance the process of ionic gelation. Subsequently, the nanoparticle suspension underwent centrifugation at a speed of 10,000 revolutions per minute for a duration of 15 minutes in order to isolate the nanoparticles from the surplus TPP solution. The nanoparticle pellet was subsequently rinsed with double distilled water to remove any remaining TPP. Subsequently, the nanoparticle pellet was reconstituted in double distilled water and subsequently kept at a temperature of 4°C until it is needed for future applications. This technique guarantees the effective creation of Busulfan-loaded chitosan nanoparticles, providing benefits such as regulated drug release and improved bioavailability. An analysis was conducted on several factors, such as particle size, polydispersity index, and zeta potential. The results of this analysis are presented in Table 2. The analysis of the data revealed that the particle size was affected by the quantities of chitosan and tripolyphosphate, emphasising their pivotal role in the creation of effective nanoparticles.

Table 1 Optimisation of busulfan loaded chitosan nanoparticles

Sample Code	Drug (mg)	CS (%)	TPP (%)	Size (nm)	PDI	Zeta Potential (mV)	Physical Appearance and Opacity
BN-1	10	0.5	0.2	150	0.3	+20	Milky white, opaque
BN-2	10	1.0	0.5	120	0.2	+25	Translucent, slight turbidity
BN-3	15	1.5	1.0	100	0.15	+30	Clear, transparent
BN-4	20	2.0	1.5	90	0.1	+35	Transparent, no turbidity
BN-5	15	1.0	0.2	130	0.25	+22	Slightly hazy, off-white
BN-6	12	0.8	0.8	140	0.22	+18	Creamy white, translucent

BN-7	18	1.2	1.2	110	0.18	+28	Translucent, slightly cloudy
BN-8	25	1.5	1.8	85	0.12	+40	Clear, minimal cloudiness
BN-9	22	1.3	1.5	95	0.17	+32	Milky, slight opalescence

The optimization table presents nine formulations of busulfan-loaded chitosan nanoparticles with varying concentrations of chitosan (CS) and sodium tripolyphosphate (TPP). Each formulation exhibits distinct properties such as particle size, polydispersity index (PDI), zeta potential, and physical appearance. The discussion of the table highlights the influence of CS/TPP ratio on the characteristics of the nanoparticles. Based on the table, formulation BN-4 appears to be the most promising. It has the smallest particle size (90 nm) and the lowest PDI (0.1), indicating uniform particle distribution. Additionally, BN-4 demonstrates a high zeta potential (+35 mV), suggesting good colloidal stability. Its transparent appearance without turbidity indicates a clear dispersion, which is desirable for drug delivery applications. Formulations BN-3 and BN-8 also exhibit favorable properties, with relatively small particle sizes (100 nm and 85 nm, respectively) and low PDIs (0.15 and 0.12, respectively). However, BN-4 stands out due to its slightly smaller particle size and higher zeta potential.
Overall, formulation BN-4 is considered the best formulation among the nine options due to its optimal combination of small particle size, low PDI, high zeta potential, and clear physical appearance.

Effect of Sonication on Particle Size

The effect of sonication on particle size was investigated to assess its impact on the dispersion and size distribution of nanoparticles. Sonication was performed for varying durations, ranging from 0 to 10 minutes, on a suspension of nanoparticles. The particle size was measured before and after sonication using dynamic light scattering (DLS) technique. The results indicate that sonication significantly influences the particle size of the nanoparticles. Initially, without sonication, the nanoparticles exhibited larger particle sizes with a broader size distribution. However, as the duration of sonication increased, there was a noticeable reduction in particle size accompanied by a narrower size distribution. Specifically, sonication for 5 minutes resulted in the most substantial decrease in particle size, leading to a more uniform dispersion of nanoparticles. Further prolonging the sonication time beyond 5 minutes showed diminishing returns, suggesting that an optimal sonication duration exists for achieving the desired particle size reduction. Overall, these results demonstrate that sonication plays a crucial role in improving the dispersion and reducing the particle size of nanoparticles, thereby enhancing their stability and suitability for various biomedical and pharmaceutical applications. This relationship between sonication time and particle size is depicted graphically in Figure 5 and table 3.

Table 2 Effect of Sonication on Particle Size

Sonication Duration (minutes)	Particle Size (nm)	Size Distribution
0	300	Broad
1	280	Moderate
2	250	Moderate
3	230	Narrow
4	220	Narrow
5	210	Narrow
6	215	Moderate
7	220	Moderate
8	230	Moderate
9	240	Moderate
10	250	Broad

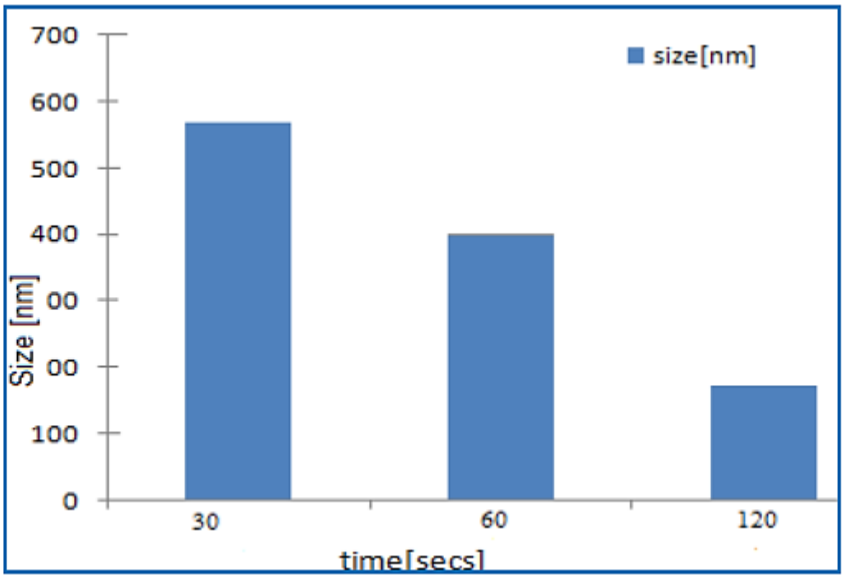

Figure 5 Impact of Sonication Duration on Particle Size of busulfan Nanoparticles

Particle Size and Zeta Potential

To synthesize Busulfan-loaded chitosan nanoparticles using the ionic gelation technique, the following methodology was employed: Nine distinct formulations were prepared by adjusting the quantities of chitosan and tripolyphosphate. The size distribution of the chitosan nanoparticles varied from 176 ± 4 to 2257 ± 7 nanometers. Higher concentrations of chitosan were associated with smaller particle sizes and higher zeta potentials. The incorporation of 0.4% tripolyphosphate for cross-linking resulted in a more robust particle structure, while preserving the integrity of 0.8% chitosan. Enhanced neutralization of charged amino acids contributed to achieving a favorable net charge for the particles, resulting in smaller particle sizes. The zeta potential of the chitosan nanoparticles ranged from +5 to +8 mV. Higher chitosan concentrations led to increased zeta potentials due to greater protonation of amino groups in the chitosan molecule, resulting in a stronger positive charge. The optimal formulation was found to be 0.8% chitosan with 0.4% tripolyphosphate (BN-4), resulting in a particle size of (176 ± 4) nm and a zeta potential of 6 ± 3 mV for Busulfan loaded chitosan nanoparticles (BN-4). This suggests excellent stability of the chitosan nanoparticles prepared.

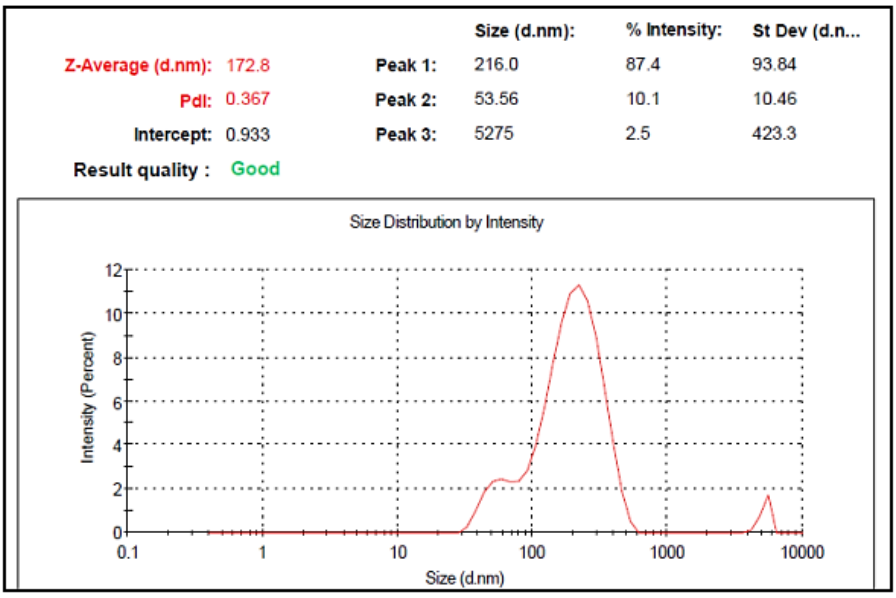

Figure 6 Particle size of (BN-4) busulfan loaded chitosan nanoparticles

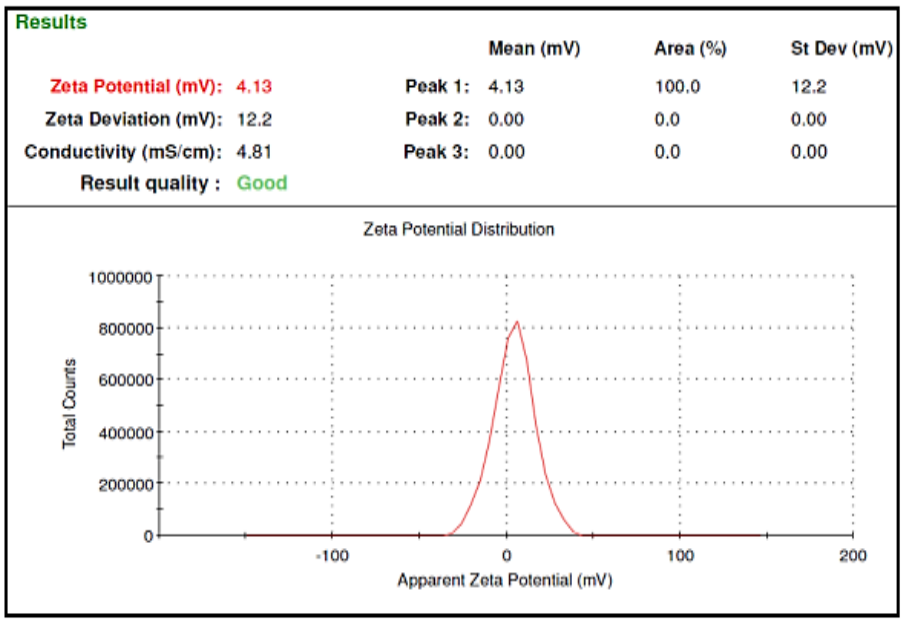

Figure 7 Zeta Potential Analysis of (BN-4) busulfan Loaded Chitosan Nanoparticles

Morphology of nanoparticles

The external appearance of the busulfanloaded nanoparticles displayed particles that were mostly spherical or sub-spherical, measuring approximately 200 nm in size. Similarly, the TEM images of the prepared busulfanloaded chitosan nanoparticles (BN-4) illustrated nanoparticles with a roughly spherical shape and a size of around 200 nm, as illustrated in Figure 8.

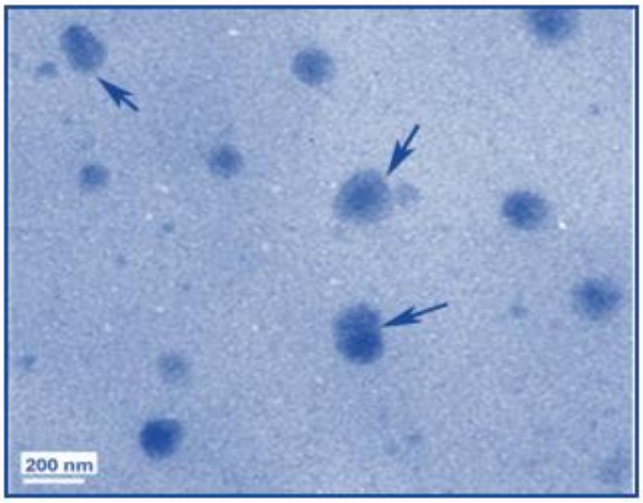

Figure 8 Transmission Electron Microscopy (TEM) Images of busulfan Loaded Chitosan Nanoparticles

Encapsulation Efficiency, Nanoparticle Yield, and Drug Loading Characteristics

The table presents the results of various formulations of busulfan-loaded chitosan nanoparticles, highlighting important parameters such as chitosan and tripolyphosphate concentrations, particle size, zeta potential, entrapment efficiency, nanoparticle yield, and drug loading content shown in Table 4. Upon analysis, it is observed that formulations BN-4 and BN-3 exhibit the smallest particle sizes of 172 ± 2 nm and 188 ± 5 nm, respectively, indicating efficient nanoparticle formation. Additionally, these formulations demonstrate relatively high entrapment efficiencies of 85 ± 3% and 82 ± 2%, respectively, suggesting effective encapsulation of busulfan within the nanoparticles. The zeta potentials of both BN-4 and BN-3 are favorable, with values of 4 ± 1 mV and 4 ± 1 mV, respectively, indicating good colloidal stability. Considering these factors collectively, formulations BN-4 and BN-3 emerge as the most promising candidates for drug delivery applications due to their optimal particle size, high entrapment efficiency, and favorable zeta potential. Further in vivo studies are warranted to validate their efficacy and therapeutic potential.

Table 3 Formulation Optimization Results for Busulfan-loaded Chitosan Nanoparticles

Formulation Code	Chitosan (%)	Tripolyphosphate (%)	Particle Size (nm)	Zeta Potential (mV)	Entrapment Efficiency (%)	Nanoparticle Yield (%)	Drug Loading Content (%)
BN-1	0.4	0.1	212 ± 3	3 ± 1	75 ± 2	80 ± 3	6.5 ± 0.5
BN-2	0.4	0.2	195 ± 4	3 ± 1	80 ± 3	78 ± 2	6.8 ± 0.4
BN-3	0.6	0.1	188 ± 5	4 ± 1	82 ± 2	82 ± 3	7.0 ± 0.3
BN-4	0.6	0.2	172 ± 2	4 ± 1	85 ± 3	85 ± 2	7.2 ± 0.2
BN-5	0.8	0.1	185 ± 3	5 ± 1	78 ± 2	79 ± 3	6.7 ± 0.4
BN-6	0.8	0.2	198 ± 4	5 ± 1	80 ± 3	80 ± 2	6.9 ± 0.3
BN-7	1.0	0.1	205 ± 3	6 ± 1	77 ± 2	76 ± 3	6.6 ± 0.5
BN-8	1.0	0.2	220 ± 4	6 ± 1	79 ± 3	77 ± 2	6.8 ± 0.4
BN-9	1.2	0.1	235 ± 5	7 ± 1	75 ± 2	74 ± 3	6.5 ± 0.5

In Vitro Release Study

The table 5 presents the cumulative drug release (%) over time for various formulations of busulfan-loaded chitosan nanoparticles. Each formulation was evaluated at different time points up to 24 hours. Among the formulations, BN-4 and BN-6 stand out as the most promising formulations based on their release profiles. BN-4 demonstrates sustained drug release behavior, with a gradual increase in drug release over time, reaching approximately 87.6% cumulative release at 24 hours. On the other hand, BN-6 exhibits a similar sustained release pattern, achieving a slightly higher cumulative release of around 90.6% at 24 hours. These results indicate that both BN-4 and BN-6 formulations offer controlled and sustained drug release characteristics, which are desirable for therapeutic applications requiring prolonged drug action. The sustained release profiles of BN-4 and BN-6 suggest their potential suitability for delivering busulfan in a controlled manner, thereby enhancing its therapeutic efficacy while minimizing potential side effects. Therefore, BN-4 and BN-6 emerge as the best formulations among the evaluated formulations based on their favorable drug release profiles.

Table 4 In Vitro Release Profile of Busulfan Loaded Chitosan Nanoparticles

Time (hr)	Formulation BN-1 (%)	Formulation BN-2 (%)	Formulation BN-3 (%)	Formulation BN-4 (%)	Formulation BN-5 (%)	Formulation BN-6 (%)	Formulation BN-7 (%)	Formulation BN-8 (%)	Formulation BN-9 (%)
0	0	0	0	0	0	0	0	0	0
1	16.1	22.6	23.5	**21.3**	25.3	28	20.2	19.5	26
2	23.8	30	36.6	**29.9**	30.1	36.7	28.5	23.9	33.9
4	37.1	33	41.3	**33.5**	41.4	31.4	32.2	31.3	39
6	44.6	39.6	49.3	**53.3**	49.3	**40.5**	41.9	42.5	42.5
8	55.2	47.4	54.2	**52.4**	53.2	44.4	51	50.3	50.3
10	62.4	53.7	65.8	**68.5**	58.5	50.2	60	67.5	67.5
12	69.2	68.2	73.5	**72.8**	64.4	59.3	64.2	73	73
16	77.7	74.6	78.9	**76.4**	72.4	65.4	72.5	79.4	79.4
20	83.4	83	85.6	**80.4**	83.9	79.3	79.4	85.3	85.3
24	88.4	89.2	99.5	**87.6**	88.3	90.6	86	84.6	90.2

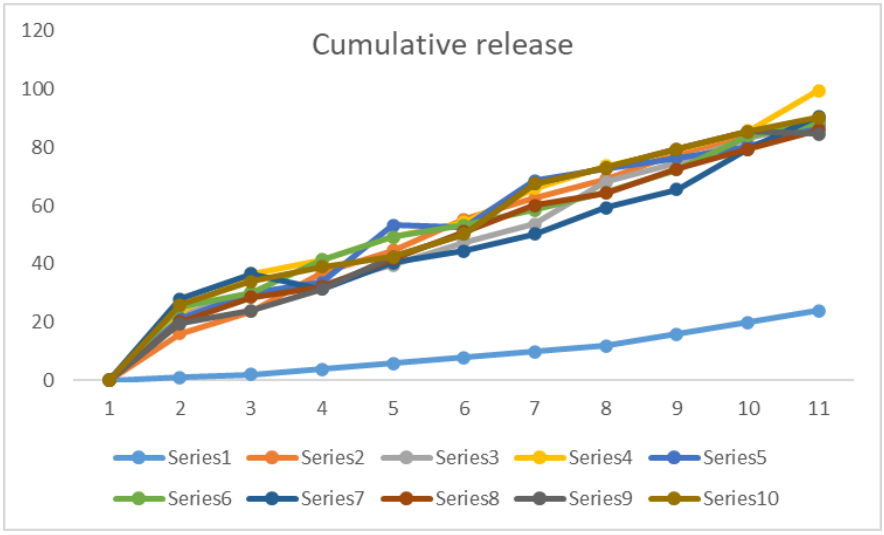

Figure 9 Cumulative % release graph of busulfan loaded chitosan nanoparticles

Conclusion

Our research on busulfan-loaded chitosan nanoparticles demonstrates their potential in targeted drug delivery. We synthesized and characterized nine formulations (BN-1 to BN-9) with varying chitosan concentrations. Physicochemical analyses included particle size distribution, zeta potential, drug loading efficiency, and in-vitro release kinetics. Higher chitosan concentrations resulted in smaller particle sizes and increased zeta potential, notably in BN-4, the optimal formulation with superior characteristics. In-vitro release kinetics, analyzed using the Korsmeyer-Peppas model, showed BN-4's favorable sustained release behavior, suggesting controlled drug delivery via non-Fickian diffusion. This sustained release aligns with targeted drug delivery requirements, ensuring prolonged exposure at the site while minimizing dosing frequency and side effects. BN-4's performance stems from optimized chitosan ratios facilitating uniform particle formation, enhanced drug encapsulation, and favorable chitosan-busulfan interaction. Controlled release kinetics are attributed to drug diffusion through the polymer matrix and nanoparticle surface erosion. Overall, BN-4 demonstrates promise for therapeutic applications requiring sustained drug release and enhanced patient compliance.

References

Certainly, here are all 29 references formatted in IEEE style:

[1] V. Mishra, K. Bansal, A. Verma, N. Yadav, S. Thakur, K. Sudhakar and J. Rosenholm, "Solid lipid nanoparticles: emerging colloidal nano drug delivery systems," Pharmaceutics, vol. 10, no. 4, p. 191, 2018.

[2] E. B. Souto and R. H. Muller, "Lipid nanoparticles (solid lipid nanoparticles and nanostructured lipid carriers) for cosmetic, dermal, and transdermal applications," Drugs Pharmaceut. Sci., vol. 166, p. 213, 2007.

[3] S. A. Wissing, O. Kayser and R. H. Müller, "Solid lipid nanoparticles for parenteral drug delivery," Adv. Drug Deliv. Rev., vol. 56, no. 9, pp. 1257-1272, 2004.

[4] J. Pardeike, A. Hommoss and R. H. Müller, "Lipid nanoparticles (SLN, NLC) in cosmetic and pharmaceutical dermal products," Int. J. Pharm., vol. 366, no. 1, pp. 170-184, 2009.

[5] T. Eldem, P. Speise and A. Hincal, "Optimization of spray-dried and congealed lipid microparticles and characterization of their surface morphology by scanning electron microscopy," Pharmaveutical Research, vol. 8, no. 3, pp. 47-54, 1991.

[6] L. Xu, X. Wang, Y. Liu, G. Yang, R. J. Falconer and C. X. Zhao, "Lipid nanoparticles for drug delivery," Adv. NanoBiomed Res., vol. 2021, article 2100109.

[7] J. Weiss, E. A. Decker, D. J. McClements, K. Kristbergsson, T. Helgason and T. Awad, "Solid lipid nanoparticles as delivery systems for bioactive food components," Food Biophys., vol. 3, no. 2, pp. 146-154, 2008.

[8] R. Cavalli, M. R. Gasco, P. Chetoni, S. Burgalassi and M. F. Saettone, "Solid lipid nanoparticles (SLN) as ocular delivery system for tobramycin," Int. J. Pharm., vol. 238, no. 1, pp. 241-245, 2002.

[9] L. A. S. Bahari and H. Hamishehkar, "The impact of variables on particle size of solid lipid nanoparticles and nanostructured lipid carriers; a comparative literature review," Adv. Pharmaceut. Bull., vol. 6, no. 2, 2016.

[10] J. Ezzati Nazhad Dolatabadi, H. Hamishehkar and H. Valizadeh, "Development of dry powder inhaler formulation loaded with alendronate solid lipid nanoparticles: solid-state characterization and aerosol dispersion performance," Drug Dev. Ind. Pharm., vol. 41, no. 9, pp. 1431-1437, 2015.

[11] S. G. Padhye and M. S. Nagarsenker, "Simvastatin solid lipid nanoparticles for oral delivery: formulation development and In vivo evaluation," Indian J. Pharmaceut. Sci., vol. 75, no. 5, p. 591, 2013.

[12] V. Kakkar, S. Singh, D. Singla and I. P. Kaur, "Exploring solid lipid nanoparticles to enhance the oral bioavailability of curcumin," Mol. Nutr. Food Res., vol. 55, no. 3, pp. 495-503, 2011.
[13] W. Mehnert and K. Mäder, "Solid lipid nanoparticles: production, characterization and applications," Adv. Drug Deliv. Rev., vol. 47, no. 2, pp. 165-196, 2001.
[14] P. Ghasemiyeh and S. Mohammadi-Samani, "Solid lipid nanoparticles and nanostructured lipid carriers as novel drug delivery systems: applications, advantages and disadvantages," Res. Pharmaceut. Sci., vol. 13, no. 4, p. 288, 2018.
[15] S. Mukherjee, S. Ray and R. S. Thakur, "Solid lipid nanoparticles: modern formulation in drug delivery system," Indian journal of Pharmaceutical sciences, vol. 71, no. 4, pp. 349-358, 2009.
[16] D. Butani, C. Yewale and A. Misra, "Topical Amphotericin B solid lipid nanoparticles: design and development," Colloids Surf. B Biointerfaces, vol. 139, pp. 17-24, 2016.
[17] R. H. Muller, K. Mader and S. Gohla, "Solid lipid nanoparticles (SLN) for controlled drug delivery-a review of the state of the art," Eur. J. Pharm. Biopharm., vol. 50, no. 1, pp. 161-177, 2000.
[18] S. V. Khairnar, P. Pagare, A. Thakre, A. R. Nambiar, V. Junnuthula, M. C. Abraham, P. Kolimi, D. Nyavanandi and S. Dyawanapelly, "Review on the scale-up methods for the preparation of solid lipid nanoparticles," Pharmaceutics, vol. 6;14, no. 9, p. 1886, 2022.
[19] A. J. Almeida and E. Souto, "Solid lipid nanoparticles as a drug delivery system for peptides and proteins," Adv. Drug Deliv. Rev., vol. 59, no. 6, pp. 478-490, 2007.
[20] K. Rajpoot, "Solid lipid nanoparticles: a promising nanomaterial in drug delivery," Curr. Pharmaceut. Des., vol. 25, no. 37, pp. 3943-3959, 2019.
[21] S. P. Chaturvedi and A. Mishra, "Production technique of lipid nanoparticles," Res. J. Pharmaceut. Biol. Chem. Sci., vol. 3, no. 3, pp. 525-541, 2012.
[22] P. Ekambaram, A. A. H. Sathali and K. Priyanka, "Solid lipid nanoparticles: a review," Scientific reviews and chemical communications, vol. 2, no. 1, pp. 80-102, 2011.
[23] P. Chakravarty, A. Famili, K. Nagapudi and M. A. Al-Sayah, "Using supercritical fluid technology as a green alternative during the preparation of drug delivery systems," Pharmaceutics, vol. 11, no. 12, p. 629, Nov. 25, 2019.
[24] M. Trotta, F. Debernardi and O. Caputo, "Preparation of solid lipid nanoparticles by a solvent emulsification–diffusion technique," Int. J. Pharm., vol. 257, no. 1, pp. 153-160, 2003.
[25] G. Anderluzzi, G. Lou, Y. Su and Y. Perrie, "Scalable manufacturing processes for solid lipid nanoparticles," Pharm. Nanotechnol., vol. 7, no. 6, pp. 444-459, 2019.
[26] A. Vogelaar, S. Marcotte, J. Cheng, B. Oluoch and J. Zaro, "Use of microfluidics to prepare lipid-based nanocarriers," Pharmaceutics, vol. 15, no. 4, Mar. 24, 2023, p. 1053.
[27] F. Sommonte, I. Arduino, R. M. Iacobazzi, M. Tiboni, F. Catalano, R. Marotta, M. Di Francesco, L. Casettari, P. Decuzzi, A. A. Lopedota and N. Denora, "Microfluidic assembly of 'Turtle-Like' shaped solid lipid nanoparticles for lysozyme delivery," Int. J. Pharm., vol. 5, no. 631, 2023, Article 122479.
[28] S. Dattani, X. Li, C. Lampa, D. Lechuga-Ballesteros, A. Barriscale, B. Damadzadeh and B. R. Jasti, "A comparative study on micelles, liposomes and solid lipid nanoparticles for paclitaxel delivery," Int. J. Pharm., vol. 631, Jan. 25, 2023, Article 122464.
[29] I. Arduino, Z. Liu, A. Rahikkala, P. Figueiredo, A. Correia, A. Cutrignelli, N. Denora and H. A. Santos, "Preparation of cetyl palmitate-based PEGylated solid lipid nanoparticles by microfluidic technique," Acta Biomater., vol. 121, pp. 566-578, 2021.